Nanomolding of Two-Dimensional Materials

Quynh P. Sam[a], Qishuo Tan[b], Christian D. Multunas[c], Mehrdad T. Kiani[a], Ravishankar Sundararaman[d], Xi Ling[b,e,f], Judy J. Cha[a]

a) Department of Materials Science and Engineering, Cornell University, Ithaca, NY
b) Department of Chemistry, Boston University, Boston, MA
c) Department of Physics, Applied Physics, and Astronomy, Rensselaer Polytechnic Institute, Troy, NY
d) Department of Materials Science and Engineering, Rensselaer Polytechnic Institute, Troy, NY
e) Division of Materials Science and Engineering, Boston University, Boston, MA
f) The Photonic Center, Boston University, Boston, MA

Abstract

Lateral confinement of layered, two-dimensional (2D) materials has uniquely enabled the exploration of several topological phenomena in electron transport due to the well-defined, nanoscale cross-sections and perimeters. At present, research on laterally confined 2D materials is constrained by the lack of synthesis methods that can reliably and controllably produce nanostructures with narrow widths and high aspect ratios. We demonstrate the use of thermomechanical nanomolding (TMNM) to fabricate nanowires of six layered materials (Te, In_2Se_3, Bi_2Te_3, Bi_2Se_3, GaSe, and Sb_2Te_3) with widths of 40 nm and aspect ratios above 100. During molding, the van der Waals (vdW) layers rotate by 90º from the horizontal direction in the bulk feedstock to the vertical direction in the molded nanowire such that the layers are aligned along the nanowire length. We find that interfacial diffusion and surface energy minimization drive the nanowire formation during TMNM, often resulting in single crystalline nanowires with consistent crystallographic orientation.

Introduction

Layered van der Waals (vdW) two-dimensional (2D) materials have been the source of major advancements across many research disciplines owing to their unique electronic[1,2], mechanical[3], and optical properties[4]. While their thickness-dependent properties have been investigated down to the monolayer limit, studies of their lateral confinement into extremely narrow nanostructures (<50 nm) are sparse. Nonetheless, laterally confined layered materials have led to important discoveries such as chiral edge channel interactions in quantum anomalous Hall insulators[5], Berry phase detection for topological surface states via Aharanov-Bohm oscillations in

topological insulators[6], and Majorana bound states that are anticipated for quantum computing[7,8,9]. Thus, lateral confinement is an effective strategy for tailoring the electronic properties of layered materials, making it a potentially transformative tool for designing next generation electronic and spintronic devices. The scarcity of lateral confinement studies stems from the lack of synthesis methods that can fabricate extremely narrow nanostructures with high aspect ratios and uniform widths. Epitaxial thin film growth techniques such as molecular beam epitaxy (MBE) can synthesize nanowires, but intensive growth optimization is needed for each material system. Other methods such as chemical vapor deposition (CVD) and vapor-liquid-solid (VLS) growth provide limited control over morphology, often resulting in layered nanomaterials with widths above 100 nm and large size distributions[10].

The recently developed nanofabrication technique of thermomechanical nanomolding (TMNM) provides a straightforward process to make narrow nanowires with high aspect ratios and uniformity. In TMNM, a bulk material of interest is extruded through a nanoporous mold at elevated temperatures (approximately $0.5T_m$, where T_m is the material's melting point in Kelvin) and pressures (higher than 100 MPa)[11]. Nanowire growth during TMNM is driven by lattice and interfacial diffusion[12] along the mold channels. Additionally, grain re-orientation occurs at the base of the nanowire in order to minimize the interfacial energy between the crystal and mold surfaces, leading to formation of single crystalline wires with consistent growth orientation[13]. TMNM is materials agnostic and has been successfully applied to metallic elements[11], alloys[14], and intermetallic compounds[15]. If TMNM can work for 2D materials, it will produce narrow, singlecrystalline nanowires of 2D materials with large aspect ratios. Due to the extremely anisotropic bonding nature consisting of weak interlayer interactions and strong in-plane bonding, however, it is unclear if TMNM can work for 2D materials.

Here, we demonstrate the successful TMNM of laterally confined nanowires of layered 2D materials with diameters of 40 nm and aspect ratios greater than 100. The vdW layers are consistently parallel to the nanowire length and molding direction even though the layers in the bulk feedstock are oriented perpendicular to the molding direction, showing that a 90° layer rotation occurs during the TMNM process. When molding is done at sufficiently high temperatures for diffusion dominated growth, the nanowires are single crystalline. We demonstrate that TMNM of layered materials is a general strategy as we successfully mold six different layered systems:

Te, In$_2$Se$_3$, Bi$_2$Te$_3$, Bi$_2$Se$_3$, GaSe, and Sb$_2$Te$_3$. Te, Bi$_2$Te$_3$, Bi$_2$Se$_3$, and Sb$_2$Te$_3$ are topological materials and have demonstrated exotic phenomena such as superconductivity[16] and topological surface-dominated transport[17] at nanoscale dimensions. GaSe and 2D ferroelectric In$_2$Se$_3$[18] exhibit size-dependent bandgaps with potential applications in optoelectronic and memory devices[19]. We show that TMNM enables fabrication of laterally confined nanowires of layered vdW materials with high aspect ratios and consistent crystallographic orientation that can be used to study emergent electronic properties.

Results and Discussion

Highly oriented Te and Sb$_2$Te$_3$ crystals purchased from 2Dsemiconductors and Funcmater and chemical vapor transport (CVT) grown α-In$_2$Se$_3$, Bi$_2$Te$_3$, Bi$_2$Se$_3$, and GaSe are used as bulk feedstock materials for molding. The Te, α-In$_2$Se$_3$, Bi$_2$Se$_3$, Bi$_2$Te$_3$, and GaSe feedstocks are high quality single crystals, while the Sb$_2$Te$_3$ crystals are polycrystalline. The crystals are molded at temperatures between 250°C – 450°C and pressures between 500 MPa – 5 GPa for 30 minutes using anodic aluminum oxide (AAO) molds with 40 nm pore size. Exact molding conditions for each material are summarized in Table S1. The molding direction is perpendicular to the vdW layer planes as illustrated by the schematic shown in Figure 1a. After molding, the AAO is etched away using hydrofluoric acid (HF) or potassium hydroxide (KOH), leaving the wires attached to the feedstock. Figure 1b shows a scanning electron microscope (SEM) image of In$_2$Se$_3$ nanowires with uniform diameters and aspect ratios above 120 after etching away the AAO mold. An atomically resolved high angle annular dark field-scanning transmission electron microscopy (HAADFSTEM) image of an In$_2$Se$_3$ nanowire shown in Figure 1c reveals that the layers are parallel to the nanowire length and molding direction, suggesting that a 90º layer rotation occurs from the bulk feedstock.
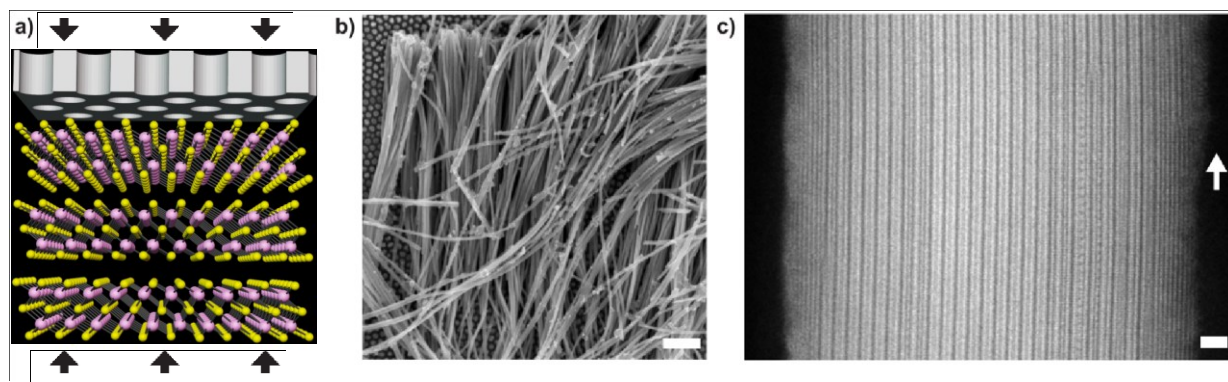

Figure 1. Overview of TMNM of 2D materials. a) Schematic of molding In$_2$Se$_3$ (In atoms in pink, Se atoms in yellow) using AAO mold (white) at high temperature and pressure. Arrows indicate the direction of applied pressure during TMNM. b) SEM image of molded In$_2$Se$_3$ nanowires with

40 nm diameter after etching AAO mold (scale bar: 1 μm). c) HAADF-STEM image of In_2Se_3 nanowire showing layers parallel to nanowire length (scale bar: 1 nm). The arrow indicates the molding direction and nanowire length with parallel vdW layer planes.

We verify the layer rotation by using focused ion beam (FIB) milling to make an electron transparent cross-section liftout of the bulk feedstock with molded nanowires attached, shown in Figure 2a. Using HAADF-STEM, we characterize the atomic structure changes from feedstock to wire. Initially, the vdW layers of the bulk In_2Se_3 crystal are oriented perpendicular to the molding direction as shown in Figure 2c. Within the molded nanowire, the vdW layers are oriented parallel to the mold direction, shown in Figure 2b. Thus, HAADF-STEM images from these regions reveal that the layers rotate 90º from the feedstock into the nanowire. We also observe that α-In_2Se_3 transitions to β-In_2Se_3 in both the feedstock and nanowire during TMNM, indicated by the centering of the middle row of Se atoms in the vdW layers as seen in the overlays in Figure 2b and 2c. This transition has been previously reported to occur at 200°C[20] and can therefore be attributed to the elevated molding temperature of 300°C. A change in stacking sequence is also observed in the HAADF-STEM images. The bulk feedstock is β-In_2Se_3 with 3R stacking where all layers are oriented in the same direction, while the nanowire has alternating 2H stacking sequence (Figure 2b and 2c).
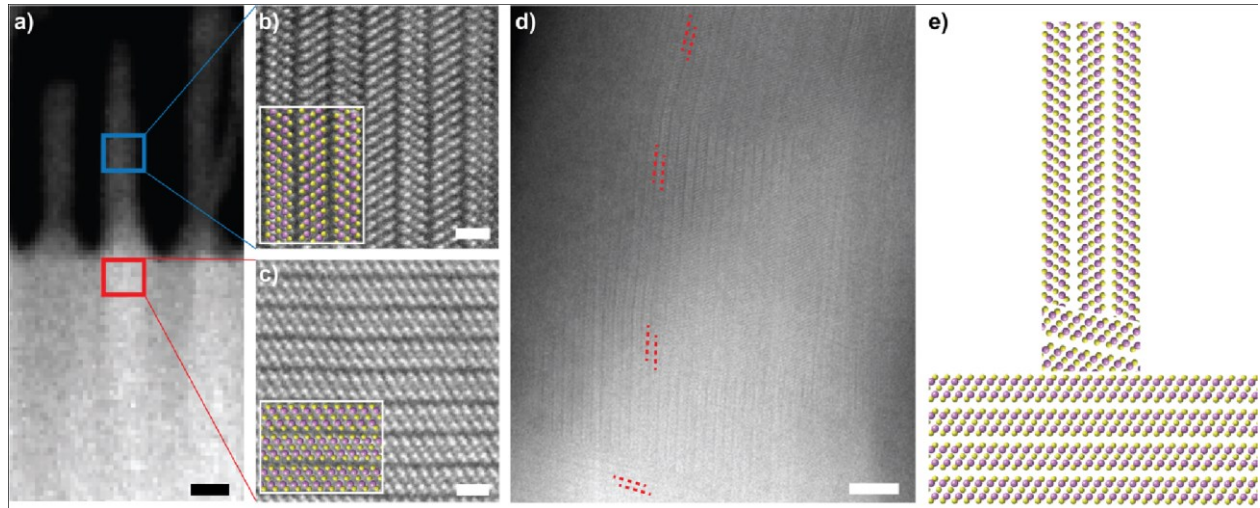

Figure 2. Characterization of layer rotation during TMNM. HAADF-STEM images of a) bulk In_2Se_3 feedstock with molded nanowires attached (scale bar: 50 nm). Atomic structure of b) molded nanowire showing β-In_2Se_3 phase with 2H stacking sequence (In atoms in pink, Se atoms in yellow, scale bar: 1 nm) and c) bulk feedstock showing β-In_2Se_3 phase with 3R stacking sequence (scale bar: 1 nm). d) Layer rotation at base of molded nanowire (scale bar: 5 nm). Red

dashed lines indicate the layer orientation direction. e) Schematic showing progression of layer orientation from bulk feedstock to molded nanowire.

The 90º layer rotation occurs beginning at the base of the nanowire as shown in Figure 2d. At the base of the nanowire, the layers begin to rotate from their initial horizontal orientation. Away from the base of the nanowire, the layers are largely parallel to the nanowire length and more subtle layer rotation occurs before the nanowire becomes completely single crystalline. These intermediate grains likely form in order to facilitate the large 90º layer re-orientation between the bulk feedstock and nanowire. The progression of layer orientation observed through HAADF-STEM imaging is illustrated by the schematic in Figure 2e. This result suggests that TMNM of 2D layered materials occurs in a similar manner to 3D crystalline materials where grain rotation occurs at the pore entrance in order to lower surface energy[11] and demonstrates that TMNM can produce nanowires of 2D materials with consistent layer orientation. To confirm that the phase of the nanowires is In_2Se_3, energy dispersive X-ray spectroscopy (EDX) is performed on both the nanowire and bulk feedstock (Figure S1). The intensity ratios of the In and Se peaks indicate that there is less In in the nanowire than the bulk crystal. This difference can be attributed to In vacancies in the nanowire resulting from the elevated molding temperature and pressure.

A major advantage of TMNM is that the size of the molded nanowires can be controlled by using AAO molds with different diameters. We mold In_2Se_3 nanowires with diameters of 80 nm and 120 nm using the same temperature, pressure, and molding duration. The AAO molds are etched and SEM is used to image the nanowires (Figure S2). The aspect ratios are approximately 130, 3.4, and 2 for the 40 nm, 80 nm, and 120 nm-diameter nanowires, respectively, showing a clear trend of decreasing length with increasing diameter. This trend indicates that interfacial diffusion of the crystal along the mold channels is one of the primary growth mechanisms, similar to the molding mechanism for 3D crystalline materials[11]. As the wire diameter decreases, the surface area to volume ratio increases, which promotes interfacial diffusion and subsequent nanowire growth during molding.

We demonstrate that TMNM can be applied to other layered materials to fabricate narrow nanowires with high aspect ratios. In contrast to MBE or CVD where growth recipes must be individually developed for each material system, TMNM is materials-agnostic and offers more straightforward parameter optimization. In addition to nanomolding of In_2Se_3, we fabricate 40 nmdiameter nanowires of 1D vdW Te and 2D vdW Bi_2Se_3, Bi_2Te_3, GaSe, and Sb_2Te_3 using TMNM.

The initial layer orientations of the bulk feedstock materials are verified by cross-section HAADFSTEM imaging (Figure S3), which shows the layers to be perpendicular to the molding direction.

After molding, the nanowires show vdW layers parallel to the nanowire length, indicating a 90° rotation from the feedstock, just like the In_2Se_3 case (Figures 3, S3, and S4). Atomic resolution STEM images confirm that the crystalline phases of the molded nanowires match those of their initial bulk feedstock materials. SEM images of Te and Bi_2Se_3 nanowires (Figures 3j and 3n) attached to the bulk feedstocks after etching the AAO mold reveal that the molded nanowires are uniform in size with high aspect ratios above 150. The nanowires bundle together during solvent drying due to cohesive forces but are easily separated via sonication for imaging and characterization. For In_2Se_3, Bi_2Se_3, and Bi_2Te_3, two different nanowire growth directions are observed: [11#00] and [1#1#20] (Figures 3 and S5). For both growth directions, the layers are oriented parallel to the length of the nanowire, suggesting that the surface energies are low and therefore accessible via TMNM. The compositions of the nanowires are analyzed using EDX to ensure that their phases match those of the initial bulk crystals (Figure S6). Te, Se, and Ga vacancies are observed in Bi_2Te_3, Bi_2Se_3, and GaSe, respectively, and can be attributed to the molding conditions. These results demonstrate the wide applicability of TMNM across many layered materials, making it a suitable technique to fabricate narrow, laterally confined nanostructures of 2D materials.
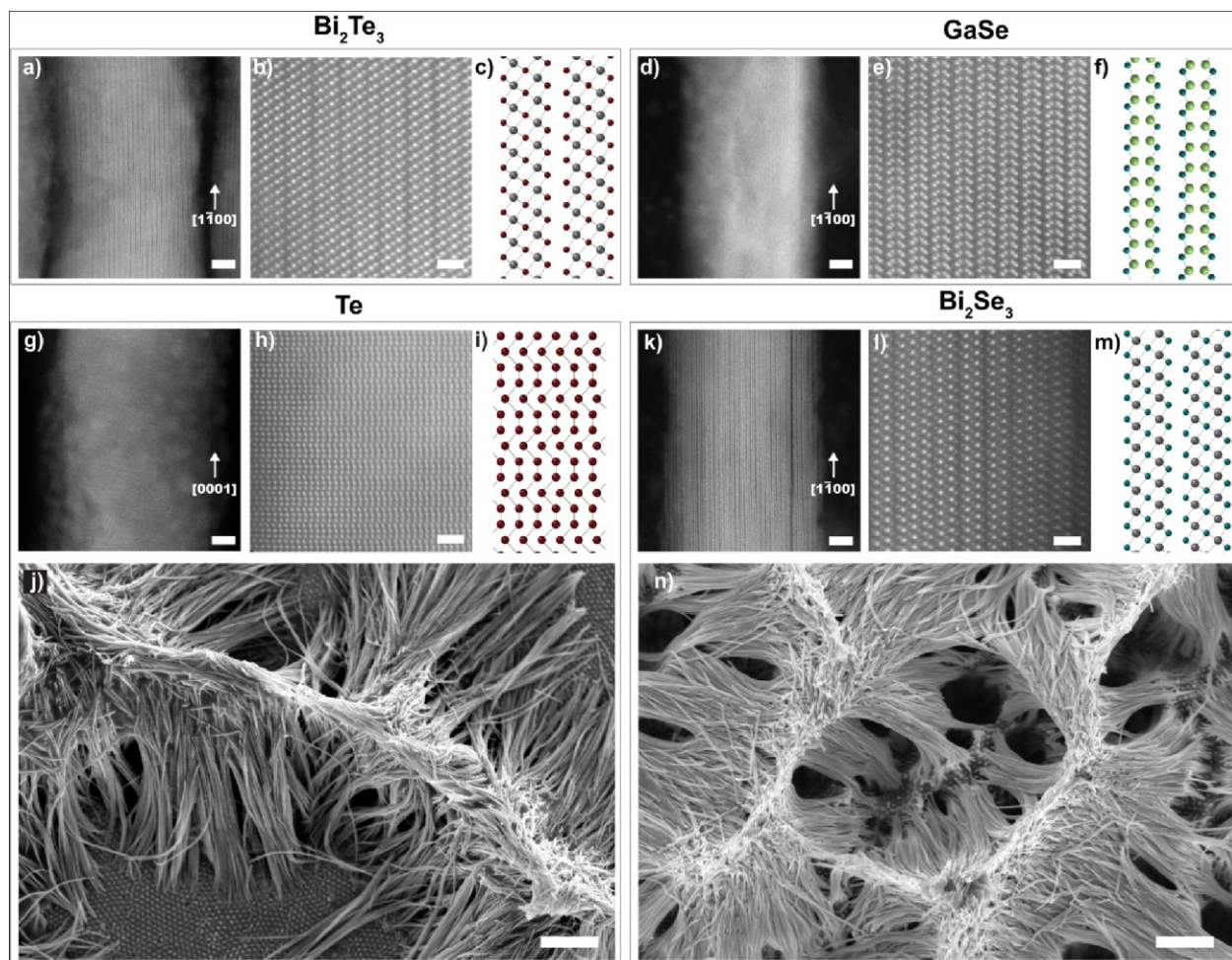
Figure 3. TMNM nanowires of various vdW materials. HAADF-STEM images and atomic structure schematics of (a-c) Bi_2Te_3 (Bi atoms in grey, Te atoms in red), (d-f) GaSe (Ga atoms in green, Se atoms in teal), (g-i) Te, and (k-m) Bi_2Se_3 (Bi atoms in grey, Se atoms in teal) with nanowire growth directions indicated by the arrows. Results for Sb_2Te_3 are shown in Figure S4. SEM images of molded j) Te and n) Bi_2Se_3 nanowires still attached to bulk feedstocks. The area at the bottom of j) is a region where the nanowires have broken off, leaving behind the hexagonally arranged pattern to reflect the location of the AAO mold pores. Scale bars are 5 nm for low magnification STEM images (a, d, g, and k), 1 nm for high magnification STEM images (b, e, h, and l), and 1 μm for SEM images (j and n).

To understand the observed layer rotation of the molded nanowires, we perform firstprinciples calculations to determine the most stable orientation for cylindrical structures of Te, In_2Se_3, Bi_2Se_3, and Bi_2Te_3. We compute surface energies for each material along the <101#0>, <0001>, <112#0>, and <101#1> directions. For Te, the (0001) surface has the highest energy, which is expected as trigonal Te chains are oriented along this direction. As such, creating this surface requires terminating the Te chains, resulting in a large surface energy. In the case of In_2Se_3, Bi_2Se_3, and

Bi$_2$Te$_3$, the [0001] direction has the lowest energy, which is expected as the layers are orthogonal to the [0001] axis. A list of all calculated surface energies for all four materials is shown in the Supplementary Information (Tables S2-S5). Using these surface energy results, we construct Wulff models for all four materials with corresponding average single-crystal surface energies (see Tables S2-S5).

While the Wulff model is useful for analysis in standard single-crystal growth, such a model becomes less practical for cylindrical nanowire geometries. Thus, we perform a geometric construction of a cylinder beyond the Wulff model for the molded nanowires. We consider a surface with its normal, n', oriented along an arbitrary direction and sample different facets to produce the lowest surface energy density. The optimized surface energy is calculated for every surface normal direction on the unit sphere. The energy of a cylinder with axis oriented along a specific direction is then determined by integrating around the sphere in directions perpendicular to the cylinder axis. Figure 4 shows the maps of surface energy density, σ, and cylindrical surface energy, $\sigma_{!"\#}$, for each material. Note that the listed Miller indices correspond to the surface normal direction for σ or the cylindrical axis orientation for $\sigma_{!"\#}$. In the case of Te, cylindrical surface energy is maximized for directions orthogonal to (0001), whereas the opposite is true for the three 2D layered materials, with surface energy being minimized in directions orthogonal to (0001). This finding agrees with the experimental observation of growth with the layers oriented parallel to the axis of the cylinder.
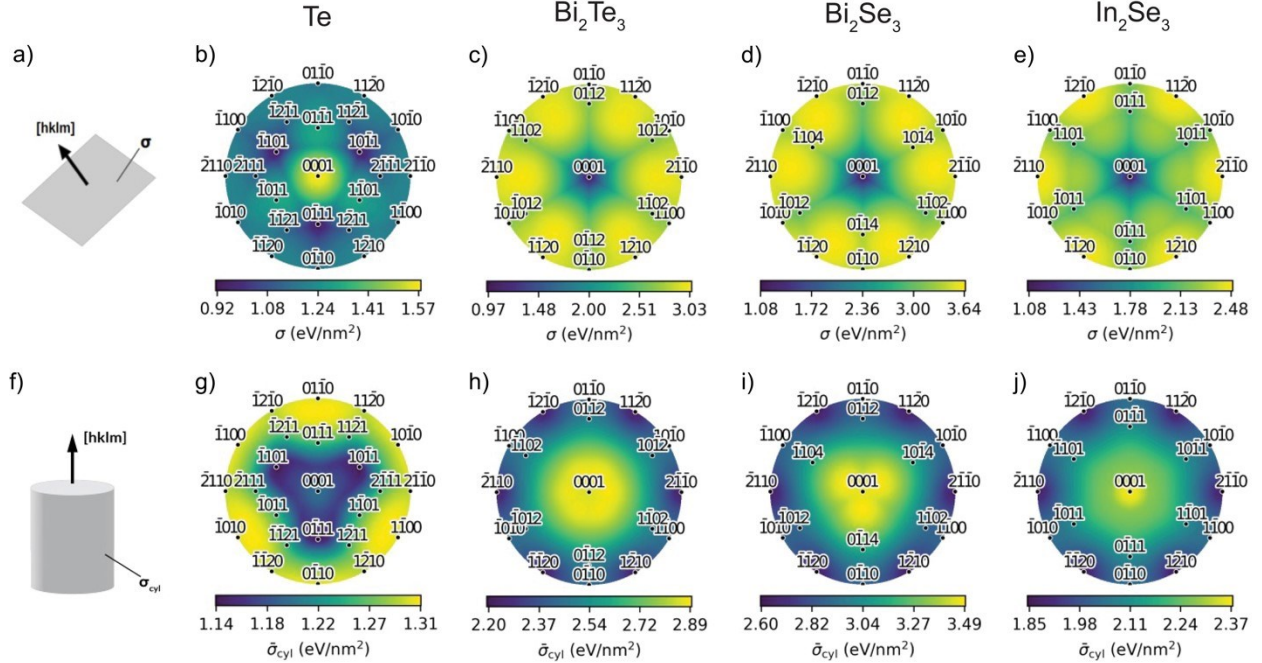
Figure 4. Computed surface energy maps for Te, Bi_2Te_3, Bi_2Se_3, and In_2Se_3. a) Schematic showing energy density of a surface with normal oriented along an arbitrary direction. Surface energy density maps for b) Te, c) Bi_2Te_3, d) Bi_2Se_3, and e) In_2Se_3. f) Schematic of cylindrical surface energy for a cylinder oriented along an arbitrary direction. Cylindrical surface energy maps for g) Te, h) Bi_2Te_3, i) Bi_2Se_3, and j) In_2Se_3. The directions on one half of the unit sphere are shown using stereographic projections.

For 3D crystals, the majority of nanowires produced by TMNM are single crystalline and defect free[21]. While the molded Te, In_2Se_3, GaSe, and Bi_2Te_3 nanowires are single crystals, we find polycrystalline nanowires for Sb_2Te_3 and Bi_2Se_3. The 90º layer rotation is still observed in the polycrystalline nanowires such that the layers are parallel to the nanowire length for the majority of the nanowire. This suggests that grain rotation occurs, but to a lesser extent, possibly due to lower atomic diffusivity. To investigate this, Bi_2Te_3 is molded at 350°C, 100°C lower than the single crystalline condition. Figure 5a shows a HAADF-STEM image of a nanowire molded at 350°C, and Figure 5b is a grain map of the nanowire showing the in-plane orientation along the nanowire length collected using 4D-STEM[22]. Grain maps showing the in-plane orientation perpendicular to the nanowire length and out of plane orientation are shown in Figure S7. The Bi_2Te_3 nanowires molded at 350°C are polycrystalline on one end which is presumed to be the nanowire base. HAADF-STEM imaging shows a grain on the polycrystalline side of the nanowire that does not have layers oriented parallel to the long axis as previously observed (Figure 5c). The grain map shows that the grains eventually rotate to become single crystalline for the majority of

the nanowire. A HAADF-STEM image from the single crystalline side of the nanowire shows the vdW layers to be oriented parallel to the nanowire length as expected (Figure 5d). At the higher molding temperature of 450°C, the Bi_2Te_3 nanowires are single crystalline throughout the entire length (Figure S8).

At low molding temperatures, the Bi_2Te_3 crystal is forced into the pore opening by the high applied pressure without exhibiting layer rotation likely due to low diffusivity, resulting in the presence of grains with vdW layers confined by the nanowire width. As the grains continue to move through the pore, interfacial diffusion and layer rotation occurs along the mold channel. The nanowire gradually becomes single crystalline with the vdW layers lying in the lowest surface energy orientation. Defects such as dislocations can be seen throughout the nanowire (Figure S9). At high molding temperature, the additional thermal energy leads to enhanced interfacial diffusion, allowing the layers to rotate to the lowest energy orientation promptly after entering the nanopores. A similar finding was observed in Ag nanowires, where increasing molding temperature from 220°C ($0.4T_m$) to 660°C ($0.76T_m$) resulted in more single crystalline nanowires[23]. These findings demonstrate that at sufficiently high temperatures, nanowire growth during TMNM can be diffusion dominated and lead to formation of single crystalline nanowires with uniform growth orientation. From this, we anticipate that the Bi_2Se_3 and Sb_2Te_3 nanowires will become single crystalline with higher molding temperatures. These findings demonstrate that TMNM can be used to create high-quality, single crystalline nanowires of 2D layered materials from both single and polycrystalline bulk feedstocks.
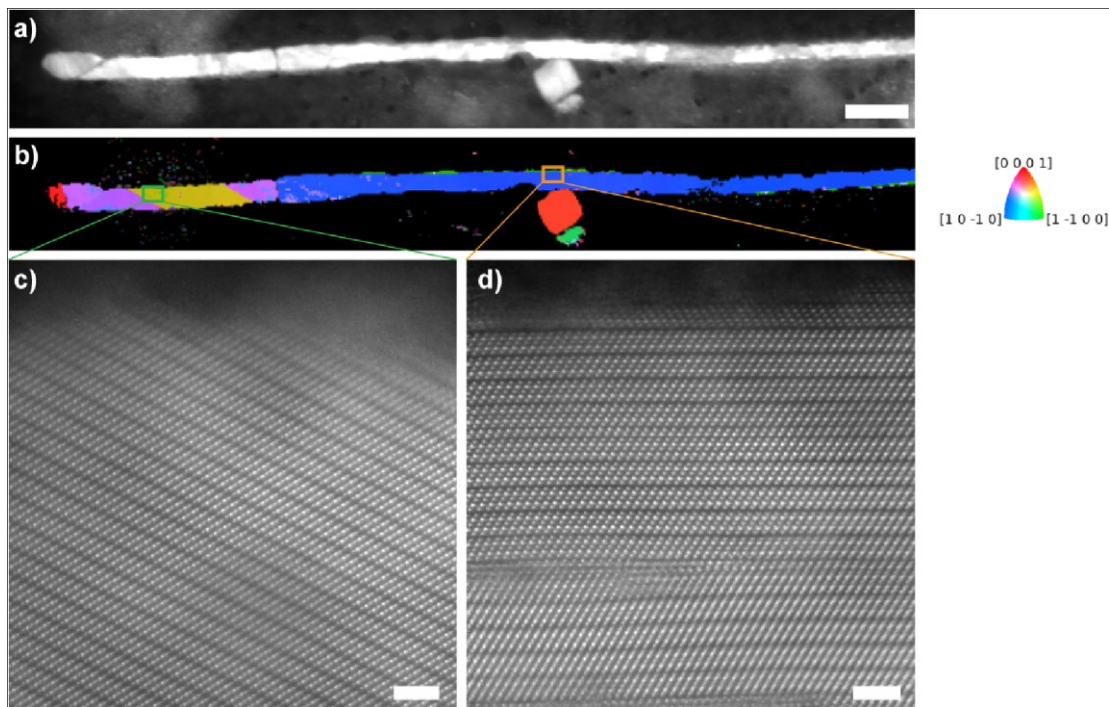
Figure 5. Microstructure characterization of a Bi_2Te_3 nanowire molded at 350°C and 5 GPa. a) HAADF-STEM image of molded Bi_2Te_3 nanowire (scale bar: 100 nm). b) 4D-STEM grain map of a). HAADF-STEM images of grains on c) polycrystalline side of nanowire showing vdW layers confined by nanowire length (scale bar: 2 nm) and d) single crystalline side of nanowire showing vdW layers oriented parallel to nanowire length (scale bar: 2 nm).

The typical molding temperatures and pressures previously used for 3D materials are approximately $0.5T_m$ and hundreds of MPa[13]. We find that much higher temperatures and pressures are necessary in order to consistently obtain more single crystalline, high aspect ratio nanowires for the 2D layered vdW materials. In_2Se_3, Bi_2Te_3, Bi_2Se_3, GaSe, and Sb_2Te_3 are molded at $0.49T_m$, $0.84T_m$, $0.74T_m$, $0.60T_m$, and $0.81T_m$, respectively (Table S1). A high pressure of 5 GPa is used to mold all compounds except for Sb_2Te_3 which is molded at 1 GPa. When TMNM is attempted with lower temperatures and pressures, molding is not consistent and usually only short wires (<1 um) are formed. The difference in homologous temperatures used for successful TMNM of the different materials suggest that In_2Se_3 and GaSe have higher diffusivity along the AAO mold walls than Bi_2Te_3, Bi_2Se_3, and Sb_2Te_3. Additionally, the In_2Se_3, Bi_2Te_3, Bi_2Se_3, and GaSe bulk feedstocks are single crystalline while the Sb_2Te_3 feedstock is polycrystalline. Grain boundary diffusion has been shown to contribute to the growth of longer nanowires in TMNM[23], which could explain why Sb_2Te_3 molds successfully at a lower pressure. The lack of grain boundary diffusion along with strong in-plane bonding can potentially make entry of the crystal into the AAO pores and nanowire

growth more difficult compared to 3D crystal structures, necessitating higher temperatures and pressures for successful TMNM of single crystalline layered 2D materials.

Conclusion

We present TMNM as a straightforward and general strategy for fabricating laterally confined nanowires of layered 2D materials which are attractive platforms for studying emergent transport phenomena. While TMNM has been demonstrated on a wide range of 3D crystalline materials, this work provides the first mechanistic study to date of its applicability towards vdW layered materials. We find that TMNM of 2D materials proceeds in a similar manner to 3D materials where grain rotation and surface energy minimization between the crystal and mold walls control nanowire formation. Thus, TMNM is an effective tool for fabricating laterally confined layered 2D materials with high aspect ratios and consistent layer orientation.

References

1. Schaibley, J. R. *et al.* Valleytronics in 2D materials. *Nat. Rev. Mater. 2016 111* **1**, 1–15 (2016).

2. Zou, X., Xu, Y. & Duan, W. 2D materials: Rising star for future applications. *Innov.* **2**, (2021).

3. Jiang, H., Zheng, L., Liu, Z. & Wang, X. Two-dimensional materials: From mechanical properties to flexible mechanical sensors. *InfoMat* **2**, 1077–1094 (2020).

4. Ma, Q. *et al.* Tunable Optical Properties of 2D Materials and Their Applications. *Adv. Opt. Mater.* **9**, 2001313 (2021).

5. Zhou, L. J. *et al.* Confinement-Induced Chiral Edge Channel Interaction in Quantum Anomalous Hall Insulators. *Phys. Rev. Lett.* **130**, 086201 (2023).

6. Peng, H. *et al.* Aharonov–Bohm interference in topological insulator nanoribbons. *Nat. Mater. 2010 93* **9**, 225–229 (2009).

7. Heffels, D. *et al.* Robust and Fragile Majorana Bound States in Proximitized Topological Insulator Nanoribbons. *Nanomater. 2023, Vol. 13, Page 723* **13**, 723 (2023).

8. Martin, I. & Morpurgo, A. F. Majorana fermions in superconducting helical magnets. *Phys. Rev. B - Condens. Matter Mater. Phys.* **85**, 144505 (2012).

9. Stanescu, T. D. & Tewari, S. Disentangling Majorana fermions from topologically trivial low-energy states in semiconductor Majorana wires. *Phys. Rev. B - Condens. Matter Mater. Phys.* **87**, 140504 (2013).

10. Cai, Z., Liu, B., Zou, X. & Cheng, H. M. Chemical Vapor Deposition Growth and Applications of Two-Dimensional Materials and Their Heterostructures. *Chem. Rev.* **118**, 6091–6133 (2018).

11. Liu, Z., Han, G., Sohn, S., Liu, N. & Schroers, J. Nanomolding of Crystalline Metals: The Smaller the Easier. *Phys. Rev. Lett.* **122**, 36101 (2019).

12. Liu, N. *et al.* Unleashing nanofabrication through thermomechanical nanomolding. *Sci. Adv.* **7**, (2021).

13. Kiani, M. T. *et al.* Nanomolding of metastable Mo4P3. *Matter* **6**, 1894–1902 (2023).

14. Liu, Z., Liu, N. & Schroers, J. Nanofabrication through molding. *Prog. Mater. Sci.* **125**, 100891 (2022).

15. Liu, N. *et al.* General Nanomolding of Ordered Phases. *Phys. Rev. Lett.* **124**, 36102 (2020).

16. Zhao, L. *et al.* Emergent surface superconductivity in the topological insulator Sb2Te3. *Nat. Commun. 2015 61* **6**, 1–8 (2015).

17. Hong, S. S., Cha, J. J., Kong, D. & Cui, Y. Ultra-low carrier concentration and surfacedominant transport in antimony-doped Bi2Se3 topological insulator nanoribbons. *Nat. Commun. 2012 31* **3**, 1–7 (2012).

18. Cui, C. *et al.* Intercorrelated In-Plane and Out-of-Plane Ferroelectricity in Ultrathin TwoDimensional Layered Semiconductor In2Se3. *Nano Lett.* **18**, 1253–1258 (2018).

19. Rybkovskiy, D. V. *et al.* Size-induced effects in gallium selenide electronic structure: The influence of interlayer interactions. *Phys. Rev. B - Condens. Matter Mater. Phys.* **84**, 085314 (2011).

20. Küpers, M. *et al.* Controlled Crystal Growth of Indium Selenide, In2Se3, and the Crystal Structures of α-In2Se3. *Inorg. Chem.* **57**, 11775–11781 (2018).

21. Kiani, M. T. & Cha, J. J. Nanomolding of topological nanowires. *APL Mater.* **10**, 080904 (2022).

22. Savitzky, B. H. *et al.* py4DSTEM: A Software Package for Four-Dimensional Scanning Transmission Electron Microscopy Data Analysis. *Microsc. Microanal.* **27**, 712–743 (2021).

23. Wu, Y., Zhang, Y., Shui, L., Wu, J. & Liu, Z. Experimental decoding of grain boundarybased plastic deformation. *Acta Mater.* **225**, 117534 (2022).

Acknowledgements

Methods

Synthesis of bulk feedstock materials

Te was purchased from 2Dsemiconductors. Single crystals of gallium selenide (GaSe) were grown via a chemical vapor transport (CVT) technique. A stoichiometric quantity of elements (molar ratio Ga:Se = 1:1, 1 g in total) and pure iodine (around 30 mg) were sealed into a quartz ampule under pressure of < 10^{-5} hPa. Then the ampule was placed in a two-zone furnace and kept at $870 - 820°C$ for a week, with the precursor side placed in the high-temperature zone. Van der Waals GaSe single crystals were collected from low-temperature end when the ampule was cooled back to room temperature in 24 hours. Indium selenide (In_2Se_3), bismuth selenide (Bi_2Se_3), and bismuth telluride (Bi_2Te_3) were grown with the same method using temperatures of 850-800°C, 500-450°C, and 500-450°C, respectively.

The synthesized crystals were characterized by Raman spectroscopy carried out on a microRaman spectrometer (Horiba-JY T64000) (Figure S11). A 532 nm laser was used as the excitation light and the signal was collected through a ×50 long-working-distance objective. The backscattered light was dispersed with an 1800 mm^{-1} grating and measured by a liquid nitrogen cooled charge-coupled device camera.

TMNM of nanowires

AAO molds were purchased from InRedox. All materials were molded as is for 30 minutes in an Ar environment using the conditions given in the Table S1. To remove the AAO mold, Te, Bi_2Se_3, Bi_2Te_3, and GaSe were etched using 5M KOH and In_2Se_3 using 20% HF. The nanowires were then released from the feedstock by sonicating in methanol.

HAADF-STEM, EDX, and 4D-STEM sample preparation and analysis

TEM samples were made by dropcasting the sonicated nanowire solutions on lacey carbon overlaid on 300 mesh copper grids. EDX samples of the bulk crystals were prepared by sonicating the bulk crystals for 20 minutes in methanol, then dropcasting the solution onto TEM

grids. Cross-section liftouts were made using a Thermo Fisher Helios G4 UX FIB with a final mill at 2-5 kV. HAADF-STEM imaging and STEM-EDX were performed on a Thermo Fisher Spectra 300 using 300 kV accelerating voltage. 4D-STEM data was collected using an electron microscope pixel array detector (EMPAD) and analyzed using py4Dstem.

DFT surface energy calculations
All first-principles calculations were performed using the open-source plane-wave software JDFTx [https://doi.org/10.1016/j.softx.2017.10.006]. Calculations for all materials were run using the Perdew-Burke-Ernzerhof (PBE) exchange-correlation functional [https://doi.org/10.1103/PhysRevLett.77.3865] with a plane wave energy cutoff of 680 eV, and ultrasoft pseudopotentials were sourced from the GBRV library [https://doi.org/10.1016/j.commatsci.2013.08.053]. Due to the layered nature of these materials, the Van der Waals D3 correction [https://doi.org/10.1063/1.3382344] was included in all calculations. Self-consistent calculations were performed using a Gamma-cented mesh of 12x12x12 k-points to compute the bulk free energies of Te, Bi_2Se_3, Bi_2Te_3, and In_2Se_3 whereas surface-oriented slabs utilized a 12x12x1 k-point mesh. Slab geometries were constructed such that the slab thickness was approximately 30 angstroms, with a vacuum spacing of 15 Angstroms. A structural relaxation was performed iteratively for bulk and slab structures to optimize the lattice constants and atomic positions. Upon calculating surface energies for all materials, Wulff models were constructed using the WulffPack Python package [https://doi.org/10.21105/joss.01944].
Due to the topological nature of Bi_2Se_3, Bi_2Te_3, and In_2Se_3, care was taken when defining the bulk energy to be used in the surface energy calculations. For each material, the computed energy density of the (0001) surface differed when using slabs with a differing thickness, corresponding to a different number of 2D layers. This discrepancy was upwards of 10% in some cases, without the surface energy converging towards a single value. To reconcile this difference, we performed total energy calculations for slabs of 3-8 layers and used a linear regression to fit the data shown in Figure S10. The corresponding slope is the ideal bulk energy value, with the yintercept corresponding to the (0001) surface energy. Using this corrected bulk energy value provided minor variation (< 1%) for slabs with varying thickness.

Total surface energy calculations of a cylindrically shaped nanostructure
We consider a surface with its normal, n', oriented along an arbitrary direction. This surface is constructed by a linear combination of facets oriented in directions $n)_s$ which together contain net orientation n'. The choice of facets is optimized to produce the lowest surface energy density for a given n', which then corresponds to the equilibrium coexistence of facets. This optimized surface energy is calculated for every possible surface normal direction on the unit sphere. The energy of a cylinder with axis oriented along a specific direction is determined by integrating around the sphere in the directions perpendicular to the cylinder axis.